IEEE Access
Multidisciplinary | Rapid Review | Open Access Journal

Received March 29, 2019, accepted April 14, 2019, date of publication April 23, 2019, date of current version May 3, 2019.

Digital Object Identifier 10.1109/ACCESS.2019.2912898

A New Morphological Filter for Fault Feature Extraction of Vibration Signals

JIANBO YU, (Fellow, IEEE), TIANZHONG HU, (Member, IEEE), AND HAIQIANG LIU, (Member, IEEE)
School of Mechanical Engineering, Tongji University, Shanghai 201804, China

Corresponding author: Jianbo Yu (jianboyu.bob@gmail.com)

This work was supported in part by the National Natural Science Foundation of China under Grant 71777173, in part by the Fundamental Research Fund for the Central University, and in part by the Shanghai Science and Technology Commission Innovation and Technology Action Plan under Grant 17511109204.

ABSTRACT Early faults in rolling bearings tend to result in periodic impulse components in the collected vibration signals. However, these fault features are always distorted by noise interferences. Feature extraction from vibration signals is an effective means to detect early defects in rolling bearings. A new morphological filter (MF), called enhanced difference morphological filter (EDMF) is proposed for vibration signal processing and then implementing bearing fault diagnosis. EDMF is capable of depressing noise and preserving effective impulsive components, where four new basic morphological operators are integrated effectively. The experimental results on simulation and bearing vibration signals verify that EDMF is effective for defect detection of rolling bearings. The comparison results show that the new MF can extract fault features more effectively from vibration signals with much noise than other typical MFs.

INDEX TERMS Bearing fault diagnosis, fault feature extraction, vibration signal, morphological filter, impact components.

I. INTRODUCTION

Vibration signal analysis is often used as an effective method in bearing fault diagnosis. If a localized defect occurs in a rolling bearing, an impulse of short duration will be generated and this will excite resonance of the bearing in the machine. These periodic impulses in vibration signals provide an important indicator of machinery faults [1]. However, these impulses are exceedingly weak in the early phase of defects because they are inevitably overwhelmed by various noise [2], [3]. Thus, the fault feature extraction from vibration signals with heavy noise becomes an important issue in machine defect detection.

Morphological filter (MF) [4], [5] is an extremely effective tool to modify the geometry of a signal by its intersection with structure element (SE). MFs have been applied successfully in image processing and analysis. In recent years, MFs were employed for impact feature extraction from various vibration signals. In general, they concentrate on the construction of morphological operators and the selection of SE. Nikolaou and Antoniadis [6] used MF with a flat SE to analyze vibration signals. Hao and Chu [7] used morphological un-decimated wavelet for fault diagnosis. Li *et al.* [8] proposed a weighted multi-scale morphological gradient filter for defect detection of bearing. Li *et al.* [9] developed weighted multiscale MF and fractal dimension based on morphological covering technique for machinery fault diagnosis. Li *et al.* [10] proposed multiscale autocorrelation based on morphological wavelet slice for detecting fault features from bearing vibration signals. Average operator (AVG) [11] was proposed for the impulse components extraction, and the length of SE was determined by using signal noise ratio (SNR). Morphological gradient (MG) [12] operator is also developed to extract harmonic waveform in a period. The geometry of SE has a significant effect on analysis results of MF. Kurtosis is used for selection of SE [13]. Particle swarm optimization was used to setup the optimal SE by Yan and Jia [14] in their morphology operator. Wang *et al.* [15] gave a concept called 'morphogram' to setup the SE. Lv and Yu [16] developed a new MF, average combination difference morphological filter (ACDIF) to extract impulsive components from bearing vibration signals. Yu *et al.* [17] employed morphological component analysis

The associate editor coordinating the review of this manuscript and approving it for publication was Yang Li.

2169-3536 © 2019 IEEE. Translations and content mining are permitted for academic research only.
Personal use is also permitted, but republication/redistribution requires IEEE permission.
See http://www.ieee.org/publications_standards/publications/rights/index.html for more information.

to extract tool edge with continuous and complete contour. In recent years, multiscale MF [10], [18]–[20] has been applied to extract fault features at different scales, which often gives a better performance for machinery fault diagnosis. Although no prior knowledge is required for multiscale MF, the computation complexity limits its wide applications.

Because the fault signals of rolling bearing always suffer from the noise and harmonics interferences, the focus of this work is to propose a new MF, called enhanced difference morphological filter (EDMF) for defect feature extraction of vibration signals. The main contributions of the paper are as follows: (1) Four new basic morphological operators are developed to extract positive or negative impulsive components in the vibration signals; (2) To make the impact features be prominent, a new morphological operator, i.e., EDMF that combines the four new operators is further proposed to extract both positive and negative impulses of vibration signals. The results on the simulation signal and bearing vibration signals illustrate that EDMF is effective to extract periodic impulses and then to perform bearing defect detections.

The rest of this paper is organized as: The basic theory of MF is introduced in Section I. The new MF, i.e., EDMF is proposed in Section II. In Section III, the simulation signal is firstly used to verify the effectiveness of EDMF. Vibration signals from rolling bearings are further used to verify effectiveness of EDMF in Section IV. Finally, the conclusions are given in Section V.

II. ENHANCED DIFFERENCE MORPHOLOGICAL FILTER

Set theory-based mathematical morphology (MM) was initially used for image processing [21], [22]. Recently, MM has been used as a demodulation method in machinery fault diagnosis [6], [23]. The four basic morphological operators, namely erosion, dilation, opening and closing are often used for various applications. Let $f(n)$ be the signal that is the function over a domain $F = (0, 1, \cdots, N-1)$. Let $g(m)$ be the SE over a domain $G = (0, 1, \cdots, M-1)(M \leq N)$. The four operators are defined:

Erosion:

$$(f \Theta g)(n) = \min\{f(n+m) - g(m)\} \tag{1}$$

Dilation:

$$(f \oplus g)(n) = \max\{f(n-m) + g(m)\} \tag{2}$$

Opening:

$$(f \circ g)(n) = (f \Theta g \oplus g)(n) \tag{3}$$

Closing:

$$(f \bullet g)(n) = (f \oplus g \Theta g)(n) \tag{4}$$

where Θ, $\oplus$, $\circ$ and $\bullet$ denote the erosion, dilation, opening and closing operator, respectively. They are capable of picking up positive or negative impulses from vibration signals. Based on the four basic operators, these typical MFs, i.e., MG, Difference filter (DIF), opening-closing and closing-opening (OCCO) [8], [24], [25] are developed for machine fault diagnosis.

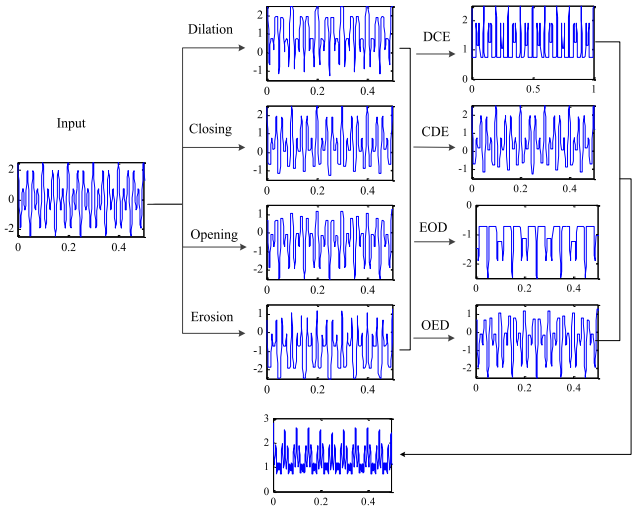

FIGURE 1. Flowchart of EDMF calculation.

In this study, four new MF operators are firstly proposed to extract positive or negative impact components of vibration signals. Then, EDMF integrates the four new operators as a new MF, which takes their own strengths in extracting impact components. Finally, it not only effectively suppresses the noise, but keeps the impact components of the vibration signals.

The EDMF calculation is shown in Fig. 1, where this simulation signal $x_0 = \cos(24\pi t) + 1.5\cos(40\pi t)$ is employed to illustrate effectiveness of EDMF for impulsive component extraction.

Considering the different effect of the four basic operators on impulse, they can be divided into two categories. One can retain the positive impulses and suppress the negative impulses: dilation and closing operator. The other can retain the negative pulse and remove the positive impulses: erosion and opening operator. Thus, these operators can be integrated to enhance the effect of positive or negative impulses in vibration signals.

Firstly, in order to extract positive impulse and keep the shape of the signal as much as possible, the cascades of dilation, closing and erosion (i.e. closing-dilation-erosion (CDE) and dilation-closing-erosion (DCE)) are defined:

$$F_{CDE}(f(n)) = (f \bullet g \oplus g \Theta g)(n) \tag{5}$$

$$F_{DCE}(f(n)) = (f \oplus g \bullet g \Theta g)(n) \tag{6}$$

Secondly, in order to extract negative impulse and keep shape of the signal as much as possible, the cascades of erosion, opening and dilation (i.e. erosion-opening-dilation (EOD) and opening-erosion-dilation (OED) are defined:

$$F_{EOD}(f(n)) = (f \Theta g \circ g \oplus g)(n) \tag{7}$$

$$F_{OED}(f(n)) = (f \circ g \Theta g \oplus g)(n) \tag{8}$$

In theory, CDE and DCE integrate the dilation and closing operators on the signal $f(n)$ to enhance the effect of suppressing the negative impulses, and the erosion operator corrects the retained positive impulses. EOD and OED integrates erosions and opening operators on the signal $f(n)$ to effectively suppress the positive impulses, and the dilation operator corrects the retained positive impulses. Thus, the four new operators, i.e., CDE, CDE, EOD and OED can enhance the ability to extract positive and negative impulses from a signal.

To extract positive and negative impact components simultaneously, the difference between F_{CDE} (F_{DCE}) and $F_{EOD}(F_{OED})$ are generated as the difference operators:

$$F_{CDE-OED}(f(n)) = (F_{CDE}(f(n)) - F_{OED}(f(n)))/2 \quad (9)$$

$$F_{DCE-EOD}(f(n)) = (F_{DCE}(f(n)) - F_{EOD}(f(n)))/2 \quad (10)$$

The difference between the two types of combined operators with different effects will further improve the ability to extract and suppress impulses from vibration signals. Finally, the average of $F_{DCE-EOD}$ and $F_{CDE-OED}$ is used as output of EDMF:

$$EDMF = \frac{F_{DCE-EOD} + F_{CDE-OED}}{2} \quad (11)$$

EDMF integrates the two new operators as a new MF, which takes their own strengths while overcoming their respective limitations for extraction of impulsive components in vibration signals. As shown in Fig. 1, the results of the CDE and DCE operators are basically positive impulses above the zero line, and it is obvious that CDE and DCE outperform the basic operators. EOD and OED can obtain the similar effect. The final result (i.e. EDMF) shows clear periodic features.

The SE setup affects performance of MF significantly. Its attributes are determined by the following three elements, i.e., shape, height and length. Generally, the shape of SE has little affection on the filtering outcome [26]. In order to simplify the calculation and preserve the shape features of a signal completely, the flat SE is used for EDMF. We define impact feature amplitude as:

$$A = (A_1 + A_2 + \ldots + A_N)/N \quad (12)$$

where A_i is the magnitude of the *ith* faulty frequency. The larger the A of the filtered signal is, the better the extracted fault feature is. Thus, the length of SE for EDMF will be setup when the used MF obtains the largest A. This indication is also used for parameter setting of SE of these comparative methods (e.g., DIF, MG, AVG and OCCO). The N is the number of the faulty frequencies considered for evaluation. As shown in Fig. 2, the sensitivity analysis of N and the best length of SE shows that the optimal length of SE tends to be stable when N reaches 5, and the filtered result is no longer affected by N. Because of the observability of spectrum analysis in the experimental section, the number of fault frequencies used for evaluation should be as small as possible. Thus, $N = 5$ is used to catch the most fault features from a vibration signal in this study.

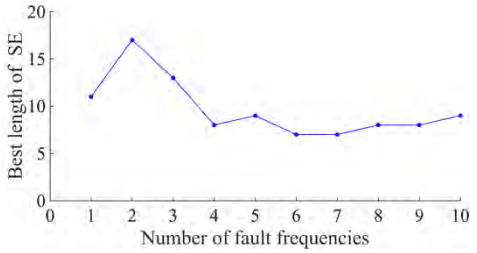

FIGURE 2. Sensitivity analysis to the number of the selected fault frequencies.

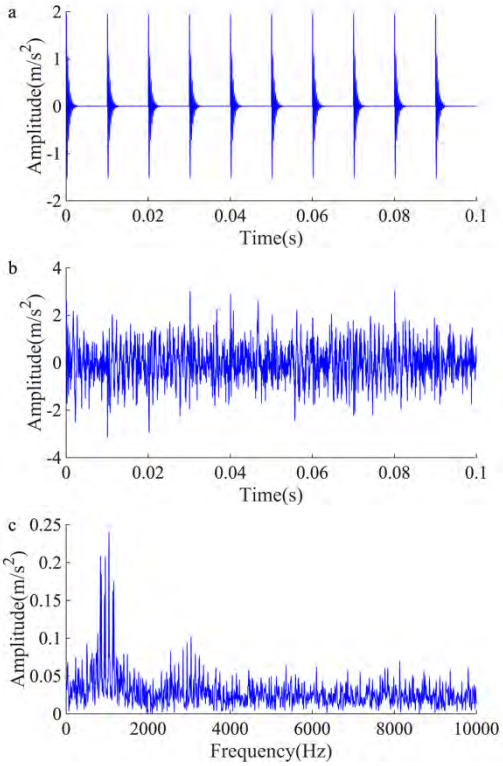

FIGURE 3. The simulation signal and its spectrum. (a) The signal without noise. (b) The signal with noise. (c) Amplitude spectrum.

III. SIMULATION SIGNAL ANALYSIS

A simulation signal is firstly employed to verify effectiveness of EDMF for impulsive feature extraction:

$$x_1(t) = 2.5e^{-10 \bmod (t/20000, 0.01)} \sin(0.3\pi t) \quad (13)$$

$$x_2(t) = 2\cos(0.2\pi t) + 2\sin(0.12\pi t) \quad (14)$$

$$x(t) = x_1(t) + x_2(t) + x_3(t) \quad (15)$$

where t is sampling point and x_1 is a periodic exponentially decaying signal with the frequency 100Hz, x_2 is the sum of two harmonic waves, and x_3 is a Gauss white noise with SNR(5dB). The sampling frequency is 20000Hz.

Fig. 3 shows this simulation signal with 2000 points and its FFT spectrum. We see that the impulsive features (i.e., Fig. 3(a)) in this simulation signal are very weak and are submerged in various interference components and noise

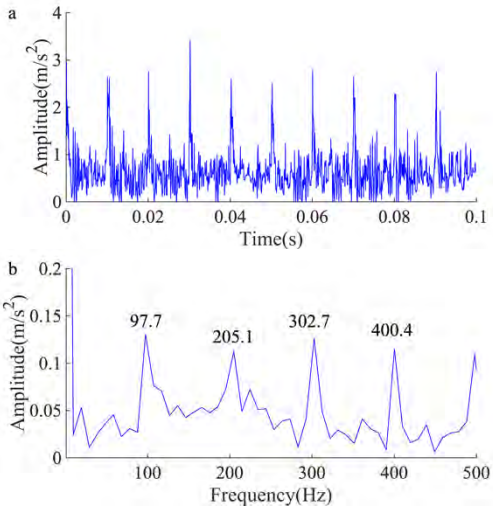

FIGURE 4. Case 1: Spectrum analysis on the filtered signal by EDMF: (a) filtered signal and (b) FFT spectrum.

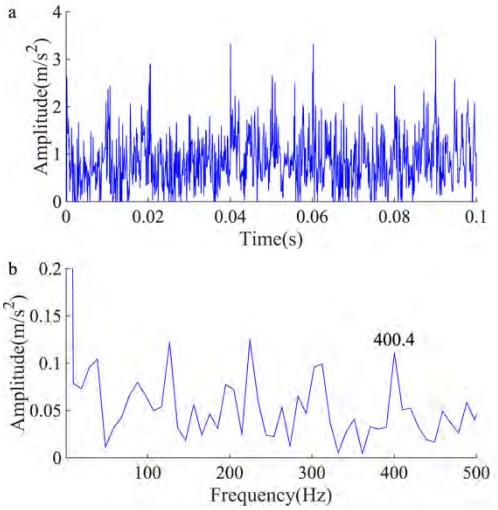

FIGURE 5. Case 1: Spectrum analysis on the filtered signal by DIF: (a) time-domain waveform and (b) FFT spectrum.

in Fig. 3(b). Thus, it is difficult to observe periodic pulses directly. It is clear that the impulsive frequency (i.e., 100Hz) as well as its multiplication frequencies (200Hz, 300Hz, etc.) cannot be detected effectively in Fig. 3(c).

EDMF is performed on this signal to extract impulsive components and simultaneously suppress interference components. The filtered signal by EDMF and the corresponding FFT spectrum are presented in Fig. 4. From Fig. 4(a), the periodical impacts become more evident on the filtered signal than that of the original signal. EDMF is capable of eliminating the harmonic components and noise interferences. Meanwhile, both of the positive and negative impulse components are well preserved. It should be noted from Fig. 4(b) that the impulsive features (97.77, 205.1, 302.7, 404.4Hz, etc.) are extracted effectively and the Gauss white noise is also eliminated effectively. The result on this simulation signal illustrates that EDMF is effective to remove the noise interferences and then extract defect features.

In order to illustrate the effectiveness of EDMF, the conventional MFs, i.e., DIF [8], [13], MG [12], AVG [11] and OCCO [25] are also performed on the simulation signal. Fig. 5-8 present the filtered results of DIF, MG, AVG and OCCO, respectively. From Figs. 5(a)-8(a), the filtered signal by DIF, MG, AVG and OCCO is still mixed with much Gaussian noise and the periodic impulses are not clear.

The corresponding FFT spectrums of these methods are presented in Figs. 5(b)-8(b). Except for MG and DIF, other MFs can not detect these defect frequencies from the signal. Moreover, we can see from Figs. 4(a)-6(a) that EDMF is more effective than MG and DIF to extract fault features, because the latter extracts only part of the impact features. These comparisons illustrate that EDMF outperforms these typical MFs, DIF, AVG, MG and OCCO that are often used for machine fault detection.

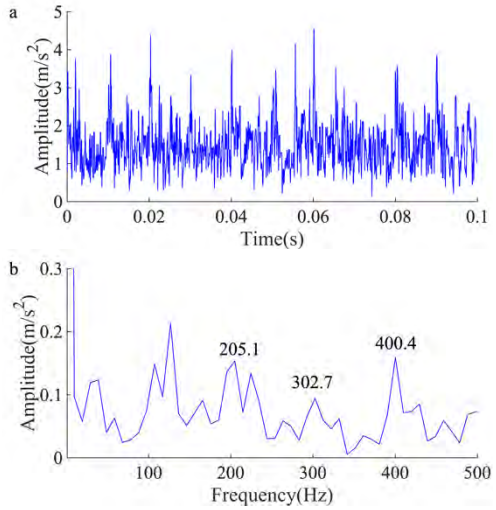

FIGURE 6. Case 1: Spectrum analysis on the filtered signal by MG: (a) filtered signal and (b) FFT spectrum.

The typical fault detection method, i.e., EMD-Hilbert [27] is also considered for comparison purpose. The generated intrinsic mode functions (IMF) by EMD are shown in Fig. 9. It is clear that the random noise as well as signal energy are concentrated in the high-frequency IMF components. Hilbert demodulation is performed on the first three IMFs selected by Kurtosis. Fig. 10 shows the filtered result of EMD-Hilbert and it is similar to the result of DIF, AVG, MG and OCCO. There is still much noise in the filtered signal in Fig. 10(a). From the FFT spectrum shown in Fig. 10(a), only the fault frequency at 205.1Hz can be extracted by EMD-Hilbert.

An effective indicator i.e., energy ration (ER) (i.e., the proportion of energy of the main defect frequencies in their respective spectrum) is further employed to evaluate

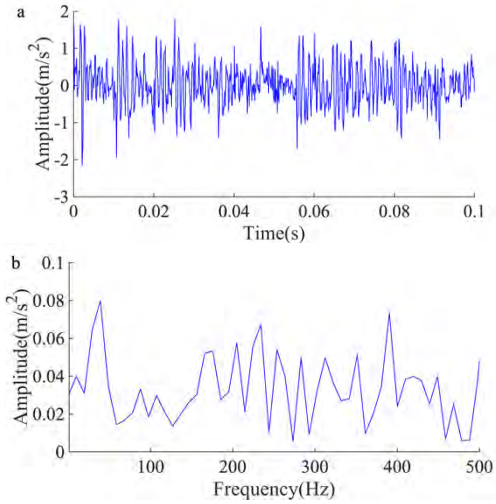

FIGURE 7. Case 1: Spectrum analysis on the filtered signal by AVG: (a) filtered signal and (b) FFT spectrum.

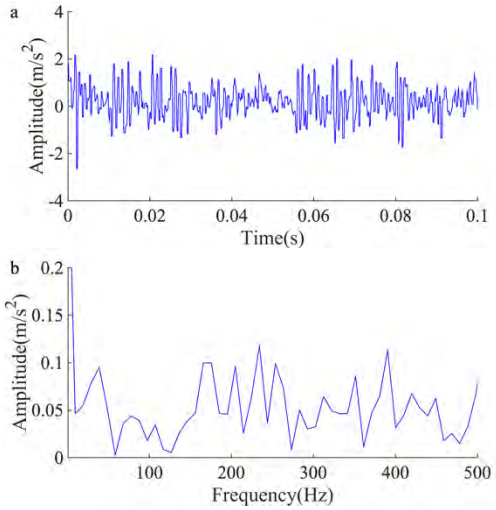

FIGURE 8. Case 1: Spectrum analysis on the filtered signal by OCCO: (a) filtered signal and (b) FFT spectrum.

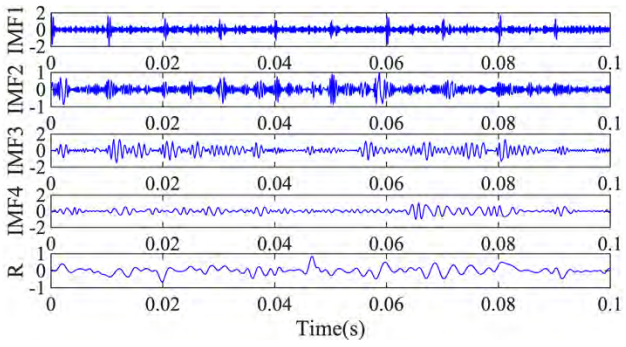

FIGURE 9. The EMD decomposition of the outer race fault signal.

effectiveness of EDMF:

$$ER = (E_1 + E_2 + \cdots + E_n)/E \tag{16}$$

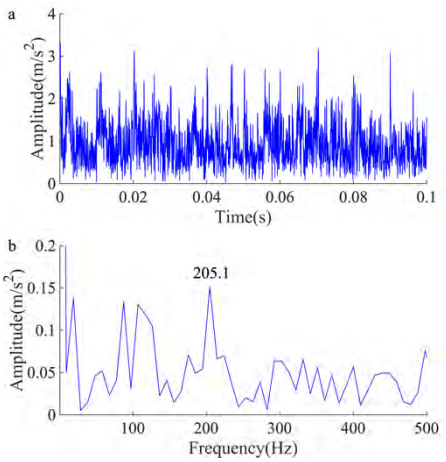

FIGURE 10. Case 1: Spectrum analysis on the filtered signal by EMD-Hilbert: (a) filtered signal and (b) FFT spectrum.

TABLE 1. Case 1: ERs (%) of EDMF, DIF, MG, AVG, OCCO and EMD-Hilbert.

EDMF	DIF	MG	AVG	OCCO	EMD-Hilbert
26.7	18.6	23.0	8.2	5.7	13.8

where $E_1 + E_2 + \cdots + E_n$ are all the energy of the defect frequency and its harmonics, and E is the total energy of the signal in the frequency band ($0 \sim 1000$ Hz). The larger the ER, the better the method. Table 1 shows ERs of these methods on the signal. EDMF with ER value of 26.7% exhibits excellent feature extraction and denoising ability. The ER values of MG, DIF and EMD-Hilbert are 23.0%, 18.6% and 13.8%, respectively, which indicates that the performance of these methods was inferior to that of EDMF. The ER values of AVG (8.2%) and OCCO (5.7%) show that noise is still dominant in the filtered signals. This comparison further illustrates that EDMF outperforms all other methods and is effective in extracting bidirectional impulses from this signal.

IV. EXPERIMENT AND RESULT ANALYSIS

A. CASE 1: BEARING WITH OUTER RACE DEFECT

In order to verify the effectiveness of EDMF to remove noise and defect feature extraction from bearing vibration signals, the vibration data collected from bearing test-bed are shown in Fig. 10. This test performed bearing run-to-failure tests under constant load conditions on a full life tester that is also produced by HBRC. The 6307-2Z single row deep groove ball bearings were tested. The load used on the bears was 12.744KN. Rolling speed (4000 r/min) and sampling frequency (20 kHz) were measured on the rolling bearings driven by AC motor. Vibration data were collected every 1 min by a data acquisition card. The bearing with outer race defect was tested. Bearing parameters and fault information (rotation frequency and fault frequency are 66.67 and 205.27 Hz respectively) are shown in Table 2.

TABLE 2. Case 1: Bearing parameters and the corresponding defect frequencies.

Load	Pitch diameter	Ball diameter	Ball number	Contact angle	f_r	f_0
12.7KN	65.5mm	15.08mm	8	0	66.67	205.27

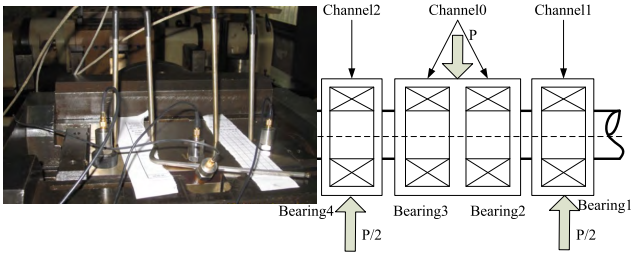

FIGURE 11. Case 1: Bearing test-bed.

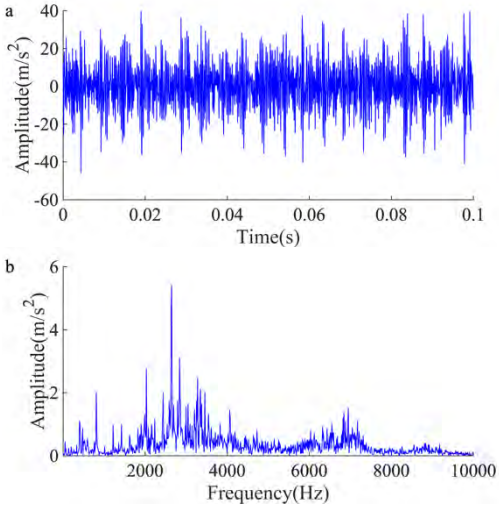

FIGURE 12. Case 1: The vibration signal and amplitude spectrum: (a) vibration signal and (b) FFT spectrum.

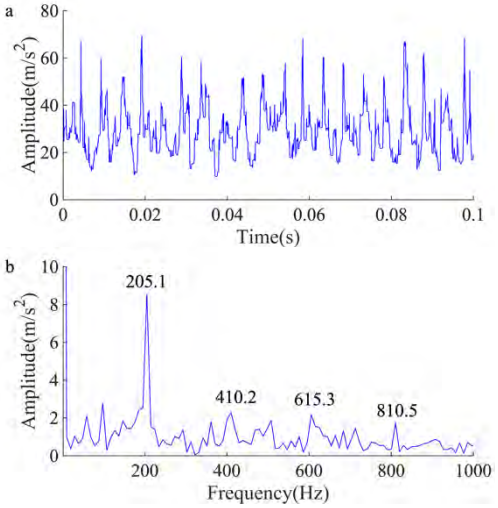

FIGURE 13. Case 1: Spectrum analysis on the filtered signal by EDMF: (a) filtered signal and (b) FFT spectrum.

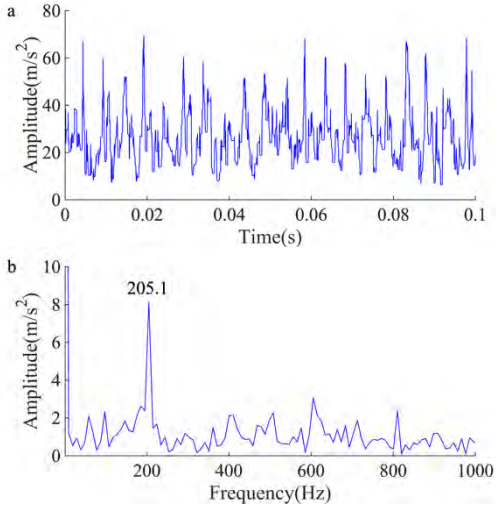

FIGURE 14. Case 1: Spectrum analysis on the filtered signal by DIF: (a) filtered signal and (b) FFT spectrum.

The vibration signal and its amplitude spectrum are presented in Fig. 12. There is obviously a large amount of noise that disturbs the defect feature information in Fig. 12(a). Moreover, it is difficult to obtain the fault frequency in the spectrum in Fig. 12(b).

The filtered signal by the EDMF and its FFT spectrum are presented in Fig. 13. The time domain graph (i.e. Fig. 13(a)) shows periodic signals, where most noise effectively can be eliminated and the impulse features can be retained by EDMF. These impact features are clear on the signal filtered by EDMF. The corresponding spectrum (i.e. Fig. 13(b)) on the filtered signal shows that the outer defect frequency 205.1Hz and its multiplication frequencies (i.e., 410.2, 615.2Hz and 810.5 Hz) are all presented. Thus, there is a good coincidence between the expected defect features of the spectrum and the actual defect features of the bearing. Both the results of noise filtering and fault feature extraction prove the effectiveness of EDMF.

To further verify the effectiveness of EDMF, Figs. 14-17 present the filtered results of DIF, MG, AVG and OCCO, respectively. Compared with EDMF, it is clear that these signals are still mixed with some noise and the periodic impulses are not clear. Their FFT spectrums (i.e. Fig. 14(b)-17(b)) can only identify fault frequencies of 205.1Hz. It is also difficult for AVG and OCCO to obtain features due to many noise interferences. These analysis results indicate that EDMF is more effective than these typical MFs, i.e., DIF, AVG, MG and OCCO.

EMD-Hilbert is finally performed on this vibration signal. A set of IMFs is generated in Fig. 18. The random noise as well as signal energy are concentrated in the high-frequency IMF components. Hilbert demodulation is performed on the

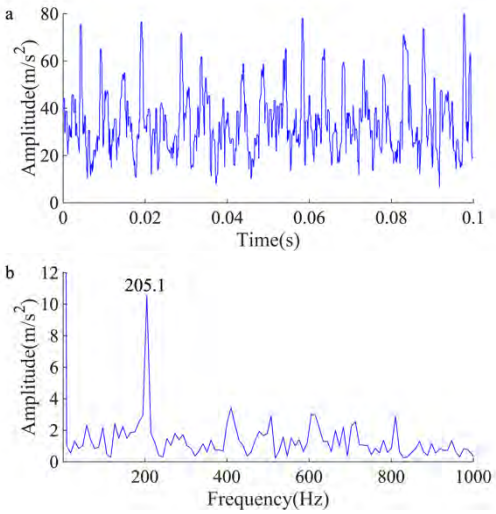

FIGURE 15. Case 1: Spectrum analysis on the filtered signal by MG: (a) filtered signal and (b) FFT spectrum.

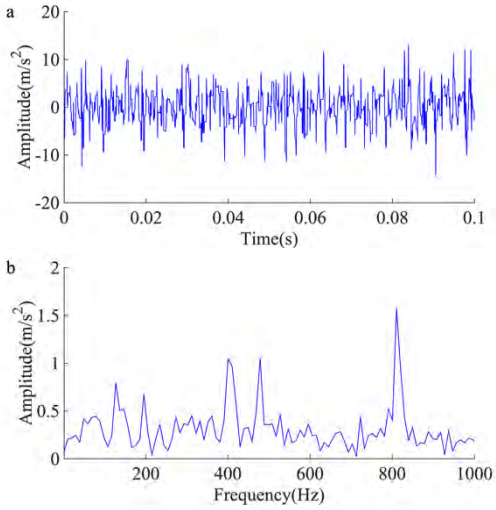

FIGURE 16. Case 1: Spectrum analysis on the filtered signal by AVG: (a) Filtered signal, and (b) FFT spectrum.

first three IMFs. The signal and its amplitude spectrums are displayed in Fig. 19. It is clear that lots of noise is still existing in the filtered signal by EMD-Hilbert. This indicates that EDMF outperforms Hilbert demodulation on this vibration signal.

To further illustrate the effectiveness of EDMF, Table 3 presents ERs of these methods on this bearing fault signal. The ERs of EDMF, DIF and MG are 39.7%, 32.2% and 36.8% respectively. Thus, EDMF is capable of extracting fault features well and reduces the noise energy greatly. The small ERs of AVG, OCCO and EMD-Hilbert confirm the analysis results in the spectrum. This ER comparison further illustrates that EDMF outperforms all other methods and is effective in extracting bidirectional impulsive components from bearing vibration signal with much noise.

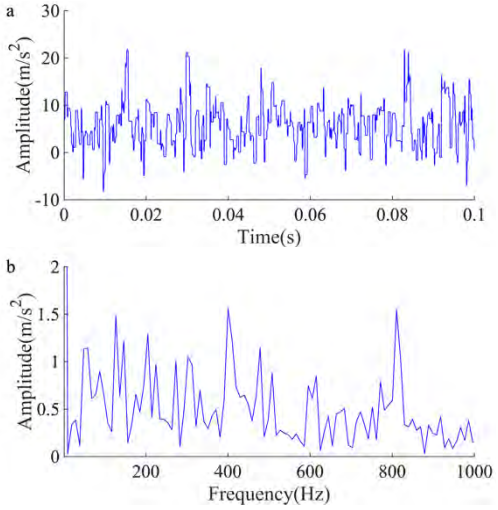

FIGURE 17. Case 1: Spectrum analysis on the filtered signal by OCCO: (a) Time-domain waveform, and (b) FFT spectrum.

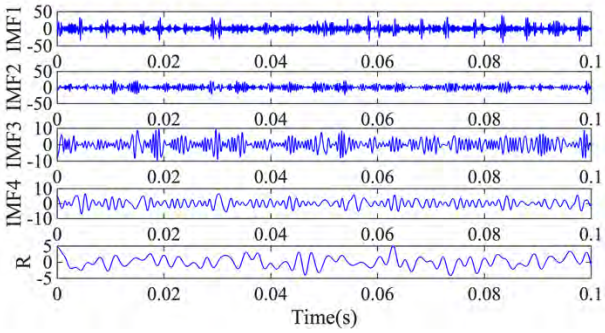

FIGURE 18. The EMD decomposition of the outer race fault signal.

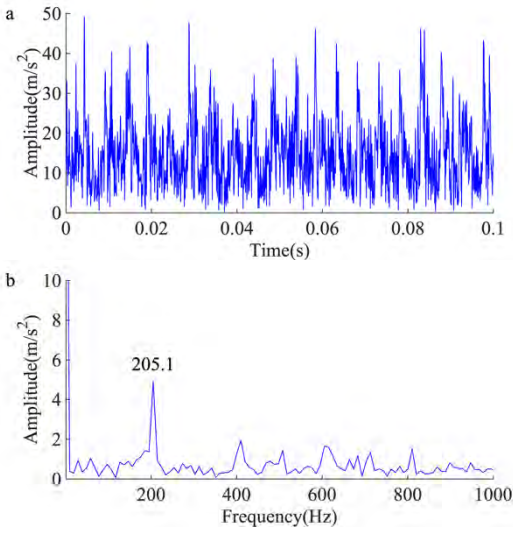

FIGURE 19. Case 1: Spectrum analysis on the filtered signal by EMD-Hilbert: (a) Time-domain waveform, and (b) FFT spectrum.

B. CASE 2: BEARING WITH INNER RACE DEFECT

The vibration signal from a bearing test-bed [28] is further considered to test performance of EDMF. Fig. 20 shows the experimental setup consisting of a Reliance Electric

TABLE 3. Case 1: ERs (%) of EDMF, DIF, MG, AVG, OCCO and EMD-Hilbert.

EDMF	DIF	MG	AVG	OCCO	EMD-Hilbert
39.7	32.2	36.8	12.3	9.0	18.5

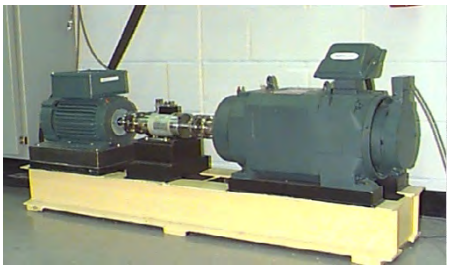

FIGURE 20. Case 2: Bearing test-bed.

TABLE 4. Case 2: Structural parameters of the bearing.

Inside diameter	Outer diameter	Thickness	Pitch diameter	Ball diameter	Ball number	Contact angle
25mm	52mm	15mm	39mm	8mm	9	0

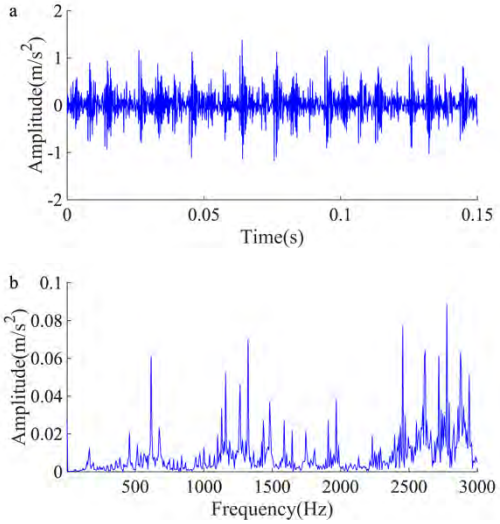

FIGURE 21. Case 2: The vibration signal and amplitude spectrum: (a) vibration signal, and (b) FFT spectrum.

2-HP motor connected to a dynamometer. The deep groove ball bearing (6205-2RS SKF) is adopted with a speed of 1797 rpm. Bearing vibration data were collected at a sampling rate of 12kHz and 2048 points were collected for each sampling at a time. Table 4 shows the bearing parameters and related information, i.e. the fault frequency (164.1 Hz) and rotation frequency (29.95 Hz) of the inner race.

Fig. 21 presents the signal and its spectrum. As can be seen from Fig. 21(b), although we can identify a defect frequency (164.1Hz) that is close to f_0, bearing fault diagnosis is confused by some interfering components that also appear in Fig. 21(a). Thus, EDMF is performed on the signal to filter the noise and extract the fault-related impulsive components.

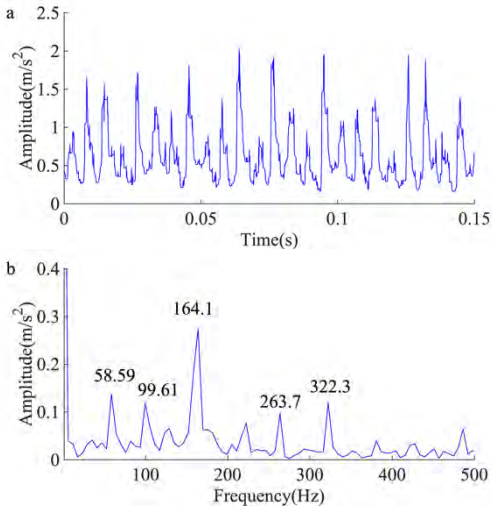

FIGURE 22. Case 2: Spectrum analysis on the filtered signal by EDMF: (a) The filtered signal, and (b) FFT spectrum.

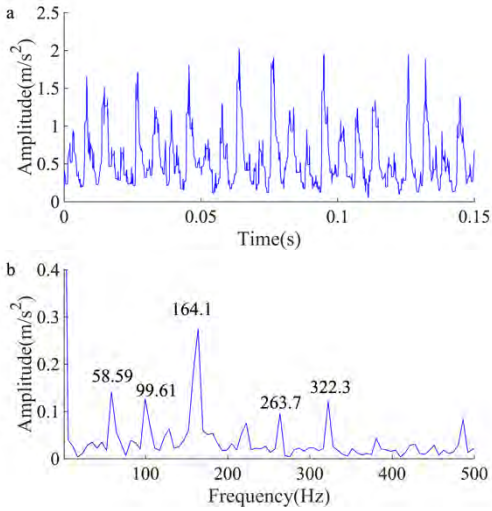

FIGURE 23. Case 2: Spectrum analysis on the filtered signal by DIF: (a) The filtered signal, and (b) FFT spectrum.

The filtered signal and its amplitude spectrum by EDMF are presented in Fig. 22, respectively. After the original signal with a lot of noise is filtered by EDMF, the signal shows clear impulsive features in Fig. 22(a). From Fig. 22(b), the defect-induced frequency(i.e. 164.1Hz) and its second harmonic (i.e., 322.3Hz) are presented clearly. In addition, 58.59Hz, 99.61Hz and 263.7Hz corresponding to $2f_r$, $4f_r$ and $4f_r + f_0$ exactly are also extracted effectively. Thus it can draw a conclusion that there is a fault defect in the inner race of the bearing and EDMF accurately extracts the fault features from the vibration signal.

The analysis results of DIF, MG, AVG, OCCO and EMD-Hilbert are also plotted in Figs. 23-26, respectively. The filtering results of DIF and MG are similar to those of EDMF, and the noise is basically eliminated, meanwhile defect frequency, rotational frequency and second harmonic are presented in

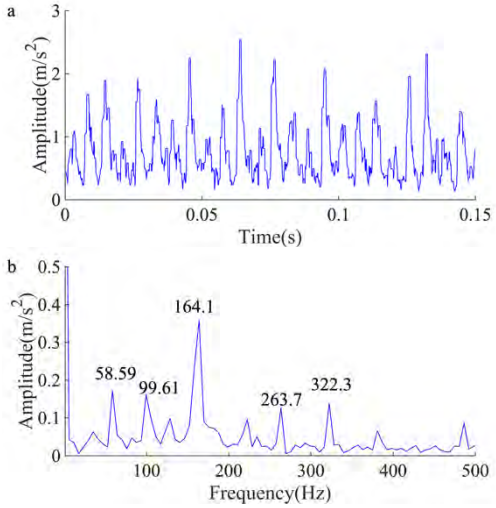

FIGURE 24. Case 2: Spectrum analysis on the filtered signal by MG: (a) The filtered signal, and (b) FFT spectrum.

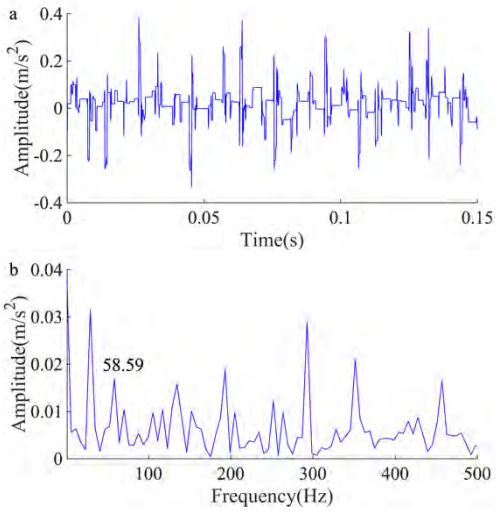

FIGURE 25. Case 2: Spectrum analysis on the filtered signal by AVG: (a) The filtered signal, and (b) FFT spectrum.

TABLE 5. Case 2: ERs (%) of EDMF, DIF, MG, AVG, OCCO and EMD-Hilbert.

EDMF	DIF	MG	AVG	OCCO	EMD-Hilbert
42.2	25.9	31.0	0.5	4.7	23.3

the FFT spectrum. As shown in Table 5, however, the ER value of EDMF(42.2%) is higher than that of DIF(25.9%) and MG(31.0%), which indicates that EDMF has better ability to eliminate noise and extract fault features. However, the ER value of AVG(0.5%) and OCCO(4.7%) are quite small. Because much noise still covers the fault information, it is difficult to carry out an accurate fault diagnosis. These results further indicate that the EDMF-based impact extraction is more effective for bearing fault diagnosis than others.

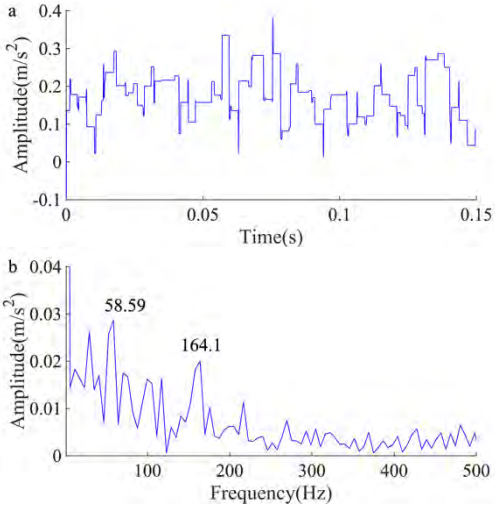

FIGURE 26. Case 2: Spectrum analysis on the filtered signal by OCCO: (a) The filtered signal, and (b) FFT spectrum.

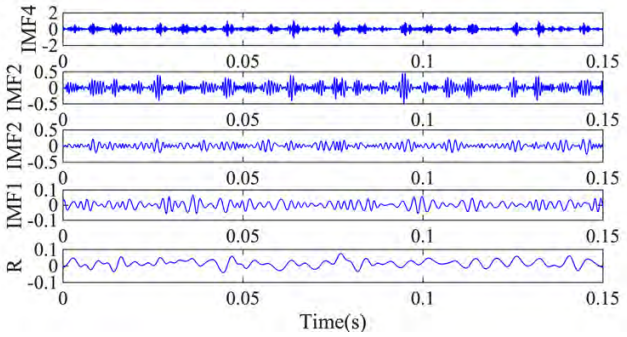

FIGURE 27. The EMD decomposition of the inner race fault signal.

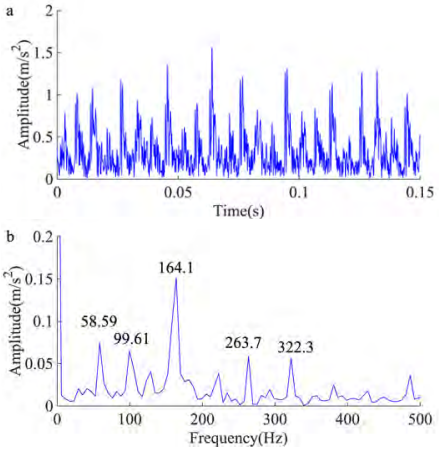

FIGURE 28. Case 2: Spectrum analysis on the filtered signal by EMD-Hilbert: (a) Results of EMD, (b) The filtered signal, and (c) FFT spectrum.

In the process of EMD-Hilbert denoising, the first three high frequency IMF components in Fig. 27 are demodulated by Hilbert to obtain the filtering results in Fig. 28. Although it also extracts fault features, it can still see a lot

of noise in Fig. 28(a). In addition, the ER value of EMD-Hilbert(23.3%) also shows that it has more noise than EDMF in the filtered signals.

V. CONCLUSIONS

The vibration signal of bearings in a machine is always influenced by various noise interferences. In this paper, a new MF called EDMF is proposed for impact component extraction from vibration signals. EDMF is capable of detecting the fault features of interest in complex working conditions that are invisible to regular MFs. The experimental results verify that EDMF is very effective for bearing defect detection. The comparison results demonstrate that EDMF outperforms these typical MFs (e.g., DIF, MG, AVG, OCCO). It has been proved that EDMF has good ability of noise elimination and fault feature extraction for vibration signal, thus it will be applied to other important mechanical components (e.g., gearbox) in the future. However, the single-scale frame in EDMF usually limits its effectiveness in fault feature extraction from bearing vibration signals. It is still difficult to setup the structure element of EDMF. An interesting studying will develop multiple-scale EDMF to solve these issues in machine fault diagnosis.

REFERENCES

[1] J. Yu and J. Lv, "Weak fault feature extraction of rolling bearings using local mean decomposition-based multilayer hybrid denoising," *IEEE Trans. Instrum. Meas.*, vol. 66, no. 12, pp. 3148–3159, Dec. 2017.

[2] C. Shen, Q. He, F. Kong, and P. W. Tse, "A fast and adaptive varying-scale morphological analysis method for rolling element bearing fault diagnosis," *Proc. Inst. Mech. Eng., Part C, J. Mech. Eng. Sci.*, vol. 227, no. 6, pp. 1362–1370, Jun. 2013.

[3] L. Meng, J. Xiang, Y. Zhong, and W. Song, "Fault diagnosis of rolling bearing based on second generation wavelet denoising and morphological filter," *J. Mech. Sci. Technol.*, vol. 29, no. 8, pp. 3121–3129, Aug. 2015.

[4] P. Maragos and R. W. Schafer, "Morphological filters–Part I: Their set-theoretic analysis and relations to linear shift-invariant filters," *IEEE Trans. Acoust., speech, signal Process.*, vol. 35, no. 8, pp. 1153–1169, Aug. 1987.

[5] P. Maragos and R. W. Schafer, "Morphological filters-Part II: Their relations to median, order-statistic, and stack filters," *IEEE Trans. Acoust., speech, signal Process.*, vol. 35, no. 8, pp. 1170–1184, Aug. 1987.

[6] N. G. Nikolaou and I. A. Antoniadis, "Application of morphological operators as envelope extractors for impulsive-type periodic signals," *Mech. Syst. Signal Process.*, vol. 17, no. 6, pp. 1147–1162, Nov. 2003.

[7] R. Hao and F. Chu, "Morphological undecimated wavelet decomposition for fault diagnostics of rolling element bearings," *J. Sound Vibrat.*, vol. 320, nos. 4–5, pp. 1164–1177, Mar. 2009.

[8] B. Li, P. L. Zhang, Z. J. Wang, S. S. Mi, and D. S. Liu, "A weighted multi-scale morphological gradient filter for rolling element bearing fault detection," *ISA Trans.*, vol. 50, no. 4, pp. 599–608, Oct. 2011.

[9] B. Li, P. Zhang, S. Mi, Y. T. Zhang, and D. S. Liu, "Multi-scale fractal dimension based on morphological covering for gear fault diagnosis," *Proc IMechE, Part C, J Mech. Eng. Sci.*, vol. 225, no. 9, pp. 2242–2249, Sep. 2011.

[10] C. Li, M. Liang, Y. Zhang, and S. Hou, "Multi-scale autocorrelation via morphological wavelet slices for rolling element bearing fault diagnosis," *Mech. Syst. Signal Process.*, vol. 31, pp. 428–446, Aug. 2012.

[11] Y. B. Dong, M. F. Liao, X. L. Zhang, and F. Z. Wang, "Fault diagnosis of rolling element bearings based on modified morphological method," *Mech. Syst. Signal Process.*, vol. 25, pp. 1276–1286, Nov. 2011.

[12] Z. Hu, C. Wang, J. Zhu, X. Liu, and F. Kong, "Bearing fault diagnosis based on an improved morphological filter," *Measurement*, vol. 80, pp. 163–178, Feb. 2016.

[13] A. S. Raj and N. Murali, "Early classification of bearing faults using morphological operators and fuzzy inference," *IEEE Trans. Ind. Electron.*, vol. 60, no. 2, pp. 567–574, Feb. 2013.

[14] X. Yan, and M. Jia, "Parameter optimized morphological filter-hat transform and its application in fault diagnosis of wind turbine," *J. Mech. Eng.*, vol. 52, no. 13, pp. 103–110, Jul. 2016.

[15] D. Wang, P. W. Tse, and Y. Tse, "A morphogram with the optimal selection of parameters used in morphological analysis for enhancing the ability in bearing fault diagnosis," *Meas. Sci. Technol.*, vol. 23, no. 6, Apr. 2012, Art. no. 065001.

[16] J. Lv and J. Yu, "Average combination difference morphological filters for fault feature extraction of bearing," *Mech. Syst. Signal Process.*, vol. 100, pp. 827–845, Feb. 2018.

[17] X. Yu, X. Lin, Y. Dai, and K. Zhu, "Image edge detection based tool condition monitoring with morphological component analysis," *ISA Trans.*, vol. 69, pp. 315–322, Jul. 2017.

[18] L. Zhang, J. Xu, J. Yang, D. Yang, and D. Wang, "Multiscale morphology analysis and its application to fault diagnosis," *Mech. Syst. Signal Process.*, vol. 22, no. 3, pp. 597–610, Apr. 2008.

[19] C. Li and M. Liang, "Continuous-scale mathematical morphology-based optimal scale band demodulation of impulsive feature for bearing defect diagnosis," *J. Sound Vibrat.*, vol. 331, no. 26, pp. 5864–5879, Dec. 2012.

[20] B. Li, P.-L. Zhang, Z.-J. Wang, S.-S. Mi, and Y.-T. Zhang, "Gear fault detection using multi-scale morphological filters," *Measurement*, vol. 44, no. 10, pp. 2078–2089, Dec. 2011.

[21] D. Goyal, B. S. Pabla, and S. S. Dhami, "Condition monitoring parameters for fault diagnosis of fixed axis gearbox: A review," *Arch. Comput. Methods Eng.*, vol. 24, no. 3, pp. 543–556, Jul. 2017.

[22] J. Serra, "Introduction to mathematical morphology," *Comput. Vis., Graph., Image Process.*, vol. 35, no. 3, pp. 283–305, Sep. 1986.

[23] J. Serra, "Morphological filtering: An overview," *Signal Process.*, vol. 38, no. 1, pp. 3–11, Jul. 1994.

[24] W. Jiang, Z. Zheng, Y. Zhu, and Y. Li, "Demodulation for hydraulic pump fault signals based on local mean decomposition and improved adaptive multiscale morphology analysis," *Mech. Syst. Signal Process.*, vols. 58–59, pp. 179–205, Jun. 2015.

[25] J. Wang, G. Xu, Q. Zhang, and L. Liang, "Application of improved morphological filter to the extraction of impulsive attenuation signals," *Mech. Syst. Signal Process.*, vol. 23, no. 1, pp. 236–245, Jan. 2009.

[26] R. M. Haralick, S. R. Sternberg, and X. Zhuang, "Image analysis using mathematical morphology," *IEEE Trans. Pattern Anal. Mach. Intell.*, vol. 9, no. 4, pp. 532–550, Jul. 1987.

[27] D. J. Yu, J. S. Cheng, and Y. Yang, "Application of EMD method and Hilbert spectrum to the fault diagnosis of roller bearings," *Mech. Syst. Signal Process.*, vol. 19, no. 2, pp. 259–270, Mar. 2005.

[28] *Case Western Reserve University Bearing Data Center Website[EB/OL].* (2011). [Online]. Available: http//csegroups.case.edu/bearingdata-center/pages/download-data-file

JIANBO YU (M'02–SM'05–F'09) received the B.Eng. degree from the Department of Industrial Engineering, Zhejiang University of Technology, Zhejiang, China, in 2002, the M.Eng. degree from the Department of Mechanical Automation Engineering, Shanghai University, Shanghai, China, in 2005, and the Ph.D. degree from the Department of Industrial Engineering and Management, Shanghai Jiaotong University, Shanghai, in 2009. In 2008, he was a Visiting Scholar with the Center for Intelligent Maintenance System, University of Cincinnati, Cincinnati, OH, USA. From 2009 to 2013, he was an Associate Professor with the Department of Mechanical Automation Engineering, Shanghai University. Since 2016, he has been a Professor with the School of Mechanical Engineering, Tongji University, Shanghai. His current research interests include intelligent condition-based maintenance, machine learning, quality control, and statistical analysis. He is an Editorial Board Member of *Advances in Mechanical Engineering*, the *Chinese Journal of Engineering*, and the *Journal of Advanced Manufacturing Research*.

TIANZHONG HU (M'23) received the B.Sc. degree from Tongji University, in 2017, where he is currently pursuing the master's degree. His main research interests include fault diagnosis and signal processing.

HAIQIANG LIU (M'26) received the B.Sc. degree from the Anhui University of Technology, in 2016. He is currently pursuing the master's degree with Tongji University. His main research interests include fault diagnosis and signal processing.